Journal of Power Sources 196 (2011) 6104–6109

Contents lists available at ScienceDirect

Journal of Power Sources

journal homepage: www.elsevier.com/locate/jpowsour

Direct CH_4 fuel cell using Sr_2FeMoO_6 as an anode material

Zhiming Wang, Ye Tian, Yongdan Li*

Tianjin Key Laboratory of Applied Catalysis Science and Technology and State Key Laboratory for Chemical Engineering (Tianjin University), School of Chemical Engineering, Tianjin University, Tianjin 300072, China

ARTICLE INFO

Article history:
Received 13 January 2011
Received in revised form 23 March 2011
Accepted 26 March 2011
Available online 6 April 2011

Keywords:
Solid oxide fuel cell
Anode
Double-perovskite
Electrochemical performance
Thermal expansion

ABSTRACT

A double-perovskite Sr_2FeMoO_6 (SFMO) has been synthesized with a combined citrate-EDTA complexing method. The material shows a double-perovskite structure after reduction in 5% H_2/Ar at 1100 °C for 20 h. A single fuel cell using this material as anode is constructed with the configuration of SFMO|$La_{0.8}Sr_{0.2}Ga_{0.83}Mg_{0.17}O_3$|$Ba_{0.5}Sr_{0.5}Co_{0.8}Fe_{0.2}O_3$. The cell exhibits a remarkable electrochemical activity in both H_2 and dry CH_4, respectively. With Oxygen as oxidant, the maximum power density is 863.7 mW cm^{-2} with H_2 as the fuel and 604.8 mW cm^{-2} with dry CH_4 as the fuel at 850 °C, respectively. SFMO has an almost linear thermal expansion coefficient from 30 to 900 °C and is very close to that of $La_{0.8}Sr_{0.2}Ga_{0.83}Mg_{0.17}O_3$. A durability test of the single cell indicates that SFMO is stable in dry CH_4 operation. Therefore SFMO can be recommended as a promising anode material for $LaGaO_3$-based solid oxide fuel cells operating with both H_2 and dry CH_4.

1. Introduction

Solid oxide fuel cell (SOFC) is an efficient power generator which converts the chemical energy of a fuel into electricity directly with very low environmental pollution. It has been paid considerable attention from researchers all over the world in the past few decades because the potential of being used as the next generation energy conversion device [1]. As a result of the high operation temperature, SOFC promotes rapid reaction kinetics. This makes the utilization of low-cost and more readily available hydrocarbon fuels, such as natural gas or coal gas, even with solid carbon, possible [2–8]. Inchoate systems of this type fuel cells involve the employment of a thin yttrium stabilized zirconia (YSZ) electrolyte with a Ni-YSZ cermet type anode and the application of hydrocarbon reforming mixture gas as the fuel [9]. They are predicted to gain an energetic efficiency of around 70% with large, multi-megawatt, integrated systems [10]. This efficiency can be improved further by the direct electrochemical oxidation of the hydrocarbon fuels instead of a mixed gas from internal or external reforming [2,7].

The traditional YSZ electrolyte works at a too high temperature which poses great challenges for the other materials composing the fuel cell, therefore, a great effort has been focused on the development of intermediate temperature electrolyte and fuel cells [11–13]. A composite electrolyte composed an oxygen ionic conduction solid phase and a molten carbonate phase showed promising results in intermediate temperature range [12,14–16], which arose a great potential for optimization of the anode and cathode materials according to the knowledge of catalyst and catalytic reactions. Another promising electrolyte material is $La_{0.8}Sr_{0.2}Ga_{0.83}Mg_{0.17}O_3$ (LSGM), it exhibits negligible electronic conductivity, good chemical stability over a wide oxygen partial pressure range and ionic conductivity of about 10^{-1} S cm^{-1} at 750 °C [11,13].

Recently, the state-of-art SOFC anode material is Ni based, which shows a good electrochemical performance with pure H_2 as fuel [12,17]. However, it is deactivated due to reasons such as coke formation unless a large amount of steam is added to the fuel [18] and sulfur poisoning when operated on a hydrocarbon fuel such as CH_4 [19] Therefore, there is a need for developing a new sort of SOFC anode materials with enough carbon resistance and sulfur tolerance for the direct electrochemical oxidation of hydrocarbon fuels. In order to develop alternative anode materials for the direct utilization of hydrocarbon fuels in SOFC, a number of approaches have been tried. Early experiments by Gorte and his co-workers investigated rare-earth doped ceria impregnated with CuO as the anode material for direct utilization of hydrocarbon fuels such as CH_4 and gasoline in the SOFC [3,6,7,20,21]. Their pioneering works showed the feasibility of direct electrochemical oxidation of CH_4 and other hydrocarbon fuels in SOFC, however, the catalytic activity of this material is proved to be disappointing. Another approach is using alloys, Kim et al. [22] tested Cu-Ni alloy as anode for direct oxidation of CH_4 in SOFC and their results showed a significant increase in power density and a moderate carbon deposition with time. Nikolla et al. [23] tested using Sn/Ni alloy as anode material

* Corresponding author. Tel.: +86 22 27405613; fax: +86 2 27405243.
E-mail address: ydli@tju.edu.cn (Y. Li).

0378-7753/$ – see front matter © 2011 Elsevier B.V. All rights reserved.
doi:10.1016/j.jpowsour.2011.03.053

for SOFC fed with CH_4 and isooctane, their results showed the tolerance of Ni electrocatalysts to coke formation can be enhanced significantly with introduction of a small amount of Sn to form Sn/Ni surface alloys. Also there are some researchers using anode barrier layers, Lin et al. [24] used composite of partially stabilized zirconia (PSZ) and CeO_2 as diffusion barrier layer and the results demonstrated that the stable operating parameter range of Ni-YSZ anode-supported SOFCs operating directly with CH_4 was increased.

Another important approach is to use oxygen-deficient, mixed-valent perovskite materials as anode due to their high ionic and electronic conductivity and good electrochemical activity in a reducing atmosphere. Tao and Irvine [25] reported a perovskite $La_{0.75}Sr_{0.25}Cr_{0.5}Mn_{0.5}O_{3-\delta}$ (LSCM) and used it as the anode material, their results showed that very good performance was achieved for CH_4 oxidation without using excess steam. However, this material shows a low electronic conductivity in reducing atmosphere and a low stability in a fuel containing 10% H_2S [26]. Wan et al. [27] examined LSCM impregnated with CuO then sputtered with Pt as anode material, they found that the formation of a porous film of Cu° improves the electronic conductivity of the anode, the sputtering of a small amount of Pt on the surface increases the rate of chemisorption and improves the cell performance with CH_4 as the fuel. Huang et al. [28–30] investigated a double-perovskite $Sr_2MMoO_{6-\delta}$ (M = Mg, Co, Ni) as the anode material for H_2 and CH_4 fuels in SOFC. Their results showed that $Sr_2MgMoO_{6-\delta}$ is an excellent SOFC anode material with an appreciable stability in a variety of fuels [28]. Sr_2CoMoO_6 exhibited a high cell performance in H_2 and wet CH_4 while Sr_2NiMoO_6 showed a notable power output only in dry CH_4 [30]. These results suggest that the double-perovskite type oxides have a great potential to be used as anode material for direct hydrocarbon fueled SOFCs.

Double-perovskite $Sr_2FeMoO_{6-\delta}$ (SFMO) has been investigated as a ferromagnetic material and is stable in reducing atmosphere [31,32]. SFMO also showed a good catalytic activity for methane combustion [33]. In this work, SFMO has been examined as the anode material for the direct electrochemical combustion of CH_4. The LSGM and $Ba_{0.5}Sr_{0.5}Co_{0.8}Fe_{0.2}O_{3-\delta}$ (BSCF) are used as the electrolyte and the cathode material, respectively. The results show that SFMO has a great potential for using as the anode material in intermediate temperature SOFCs both with H_2 and CH_4 as fuels.

2. Experimental

2.1. Material preparation

SFMO powder was synthesized via a combined citrate and EDTA complexing method with $(NH_4)_6Mo_7O_{24}{\cdot}4H_2O$, $Sr(NO_3)_2$ and $Fe(NO_3)_3{\cdot}9H_2O$ as the starting materials. EDTA was first dissolved in aqueous ammonia to form EDTA-$NH_3{\cdot}H_2O$ solution, then the necessary amount of $(NH_4)_6Mo_7O_{24}{\cdot}4H_2O$ was dissolved in EDTA-$NH_3{\cdot}H_2O$ solution under heating and stirring while the calculated amounts of $Sr(NO_3)_2$ and $Fe(NO_3)_3{\cdot}9H_2O$ were dissolved in deionized water to give a clear solution and then the clear solution was also added to the EDTA-$NH_3{\cdot}H_2O$ solution. After stirring for certain time, proper amount of citric acid was introduced, the mole ratio of EDTA acid:citric acid:total metal ions was controlled to be around 1:1.5:1. The pH value of the final solution was adjusted to around 6 using $NH_3{\cdot}H_2O$. The solution was then heated to approximately 95 °C to allow the chelates to undergo polyesterification as well as to remove excess water. With the evaporation of water, a yellow gel was obtained. The SFMO precursor was prepared by slowly decomposing the gel at 300 °C in air for 2 h and then calcined at 900 °C in air for 4 h to remove all the organic residues. The SFMO precursor was then pelletized and annealed at 1100 °C in a flowing 5% H_2/Ar atmosphere for 20 h to obtain a pure double-perovskite structure. The pellets were ground and ball milled into very fine SFMO powders.

For characterizing the structure and phase stability of SFMO, several additional samples were also prepared. SFMO powders were calcined at 1100 °C in air for 1 h to get one sample, named SFMO-ReO. The other sample, named SFMO-ReO-ReR was prepared by calcining SFMO-ReO at 850 °C in H_2 for 5 h.

The preparation of BSCF cathode and LSGM electrolyte materials has been described elsewhere [28,34].

2.2. Single fuel cell fabrication

The electrolyte-supported single cell was fabricated by a coating technique. SFMO and BSCF were both made into slurries with a binder (10% ethyl cellulose + 90% terpineol). SFMO slurry was coated onto one side of the 300 μm thick LSGM disk followed by firing at 1150 °C in N_2 atmosphere for 1 h. BSCF slurry was subsequently coated onto the other side and fired at 1000 °C in N_2 atmosphere for 1 h. Ag paste was coated on both sides and used as the current collector. The active surface area of the cell in each side was 0.593 cm^2.

2.3. Characterization

The powder X-ray diffraction (XRD) patterns of SFMO precursor, SFMO powder, SFMO-ReO and SFMO-ReO-ReR were recorded at room temperature using a D/max 2500 v/pc instrument (Rigaku Corp. Japan) with Cu-Kα radiation, 40 kV and 200 mA, at a scanning rate of 5 ° min^{-1}. To analyze the surface property of SFMO, X-ray photoelectron spectroscopy (XPS) was recorded using a PHI1600 XPS system with Mg-Kα radiation. Thermal expansion coefficients (TEC) of SFMO and LSGM were measured using a thermo mechanical analyzer (Diamond TMA SS6300, PerkinElmer, Inc.) in a N_2 atmosphere with a flow rate of 150 ml min^{-1} from 30 to 900 °C with a heating rate of 5 °C min^{-1}. The surface morphology of the single cell was characterized by a Hatchi S-4800 scanning electron microscope (SEM). The energy dispersive X-ray spectroscopy (EDX) linear scans were performed on the tested single cell to determining the interdiffusion of the ionic species in the SFMO-LSGM interface by using a Genesis XM2 instrument.

2.4. Fuel cell test

A homemade setup was used for the performance measurement of the single cell. The fuel cells were tested in a temperature range of 700–850 °C under atmospheric pressure. The flow rate of fuel gas (H_2 or CH_4) was 80 ml min^{-1} while the flow rate of O_2 was 100 ml min^{-1}. Before testing, the anode side of the cell was exposed to H_2 for 5 h at 850 °C to reduce the SFMO and then was switched to the fuel gas. The fuel cell *I–V* characteristics were measured by an IT-30 electronic load made by Ningbo BaTe Technology Co., Ltd., China. During a typical measurement, the cell voltage was varied from open circuit voltage (OCV) to a selected voltage with a step of 50 mV and a holding time of 15 s for each step to get a stable performance for each measured step, the selected voltage is 0.4 V in H_2 and 0.25 V in CH_4 in order to reach the peak power density.

3. Results and discussion

3.1. Structural characterization

Fig. 1 shows the XRD patterns of the SFMO precursor, SFMO powder, SFMO-ReO and SFMO-ReO-ReR samples. SFMO precursor shows the existence of the double-perovskite phase, but the major structure is $SrMoO_4$. After reducing the SFMO precursor at 1100 °C in 5% H_2/Ar for 20 h, a pure double-perovskite phase SFMO

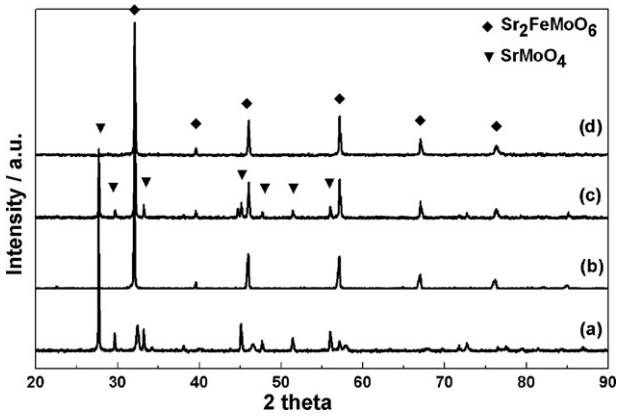

Fig. 1. XRD patterns of (a) SFMO precursor, (b) SFMO powder, (c) SFMO-ReO and (d) SFMO-ReO-ReR.

is formed (curve b, JCPDS 08-0482). The double-perovskite structure of SFMO is partly decomposed after calcination at 1100 °C in air and $SrMoO_4$ is formed again (curve c). By calcining the SFMO-ReO at 850 °C in H_2 for 5 h, the double-perovskite structure is restored. The formation of the new phase, which develops new phase boundaries and involves crystallite volume change, is unexpected in the single cell preparation because the layers and electrodes should combine well during the operation. Here, both the anode and the cathode materials, after coated on the electrolyte pellet, were fired under a N_2 atmosphere so as to prevent the possible phase changes. Before the single cell performance measurement, the multi-layered pellet was exposed in H_2 for 5 h at 850 °C to ensure a perfect SFMO structure.

3.2. Thermal expansion

An incompatibility of the thermal expansion coefficients of the SOFC component materials causes excessive thermal stress, which leads to the cracking and mechanical failure of the multi-layer, and hence reduces the lifetime of the SOFCs or even break the single cells [35]. Fig. 2 plots the thermal expansion curves of SFMO and LSGM in the temperature range of 30–900 °C in 150 ml min^{-1} N_2 gas flow. Both the two materials exhibit an almost linear thermal expansion. SFMO has an average TEC value of 14.0×10^{-6} K^{-1}, while LSGM has an average TEC value of 11.7×10^{-6} K^{-1}. Both the two expansion curves and the two average TEC values are rather close,

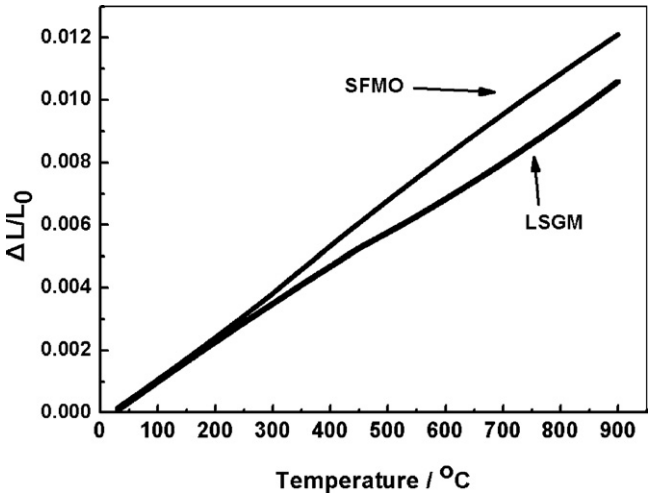

Fig. 2. Thermal expansion curves of SFMO and LSGM from 30 °C to 900 °C in N_2 atmosphere.

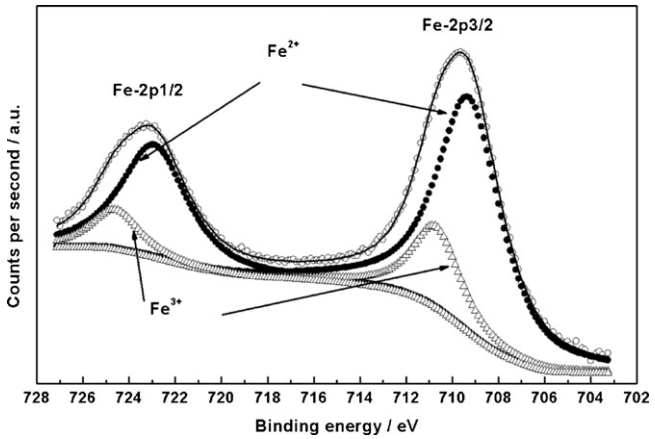

Fig. 3. Fe-2p core-level spectrum of SFMO at room temperature. (○) Measured curve; (—) fitting results of Fe-2p spectrum; (●)fitting results of Fe^{2+} contributions to the Fe-2p spectrum; (△) fitting curve of Fe^{3+} contributions to the Fe-2p spectrum.

which indicates that the SFMO and LSGM may have a good thermal compatibility in the interested temperature range.

3.3. XPS analysis

XPS spectra at room temperature were used to determine the chemical state of Fe and Mo elements in the SFMO structure by curve-fitting of the Fe-2p and Mo-3d core-level spectra. Results are shown in Figs. 3 and 4 and Table 1.

Fig. 3 shows the Fe-2p core-level spectrum at room temperature and the fitting results. The fitting curves indicate that the Fe-2p core-level spectrum consists of Fe-2p3/2 and Fe-2p1/2 excitations. The binding energies of the components extracted from the fitting curves are 709.3 eV and 710.7 eV for the Fe-2p3/2 peak and 722.9 eV and 724.6 eV for the Fe2p1/2 peak, which indicates that the Fe atoms are in different oxidation states. The contributions of ferrous (Fe^{2+}) and ferric (Fe^{3+}) states to the Fe-2p spectra are about 79.1% and 20.9%, respectively. This finding is in good agreement with the results reported by Retuerto et al. [36].

The Mo-3d core-level spectrum is shown in Fig. 4. The Mo-3d XPS spectrum presents two rather broad peaks at around 232.5 eV (3d5/2) and 235.5 eV (3d3/2) on the binding energy scale. Curve fitting of the Mo-3d spectrum yields two components, Mo^{5+} and Mo^{6+}, their binding energies are 230.8 eV and 233.6 eV for the Mo-3d5/2 peak and 232.5 eV and 235.5 eV for Mo-3d3/2 peak. The ion

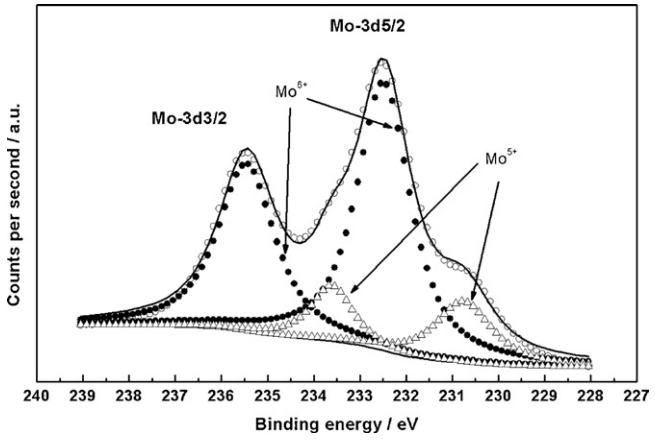

Fig. 4. Mo-3d core-level spectrum of SFMO at room temperature. (○) Measured curve; (—) fitting results of Mo-3d spectrum; (●) fitting results of Mo^{6+} contributions to the Mo-3d spectrum; (△) fitting curve of Mo^{5+} contributions to the Mo-3d spectrum

Table 1
Binding energies and valence state of Fe and Mo in SFMO double-perovskite structure (numbers in parentheses refer to the percentages of every valence state).

	Fe-2p1/2		Fe-2p3/2		Mo-3d3/2		Mo-3d5/2	
	Fe^{2+} (79.1%)	Fe^{3+} (20.9%)	Fe^{2+} (79.1%)	Fe^{3+} (20.9%)	Mo^{5+} (19.7%)	Mo^{6+} (80.3%)	Mo^{5+} (19.7%)	Mo^{6+} (80.3%)
Binding energy (eV)	722.9	724.6	709.3	710.7	232.5	235.5	230.8	233.6

concentrations extracted from the fitting curves is 80.3% for Mo^{6+} and 19.7% for Mo^{5+}, respectively, which is in good agreement with the results for Fe-2p spectra. The binding energies and the valence state of Fe and Mo in the SFMO material are summarized in Table 1.

The above mentioned XPS analysis indicates the co-existence of Fe^{3+}–Mo^{5+} and Fe^{2+}–Mo^{6+} pairs in the double-perovskite structure. The introduction of Fe^{3+}–Fe^{2+} couple not only compensates the charge balance of the double-perovskite structure but also promotes the formation of Mo^{5+}-Mo^{6+} couple, and hence increases the activity of the perovskite as Mo^{5+}-Mo^{6+} couple is thought to be the catalyst for the activation of H_2 and hydrocarbons in the double-perovskite structure [29].

3.4. SEM and EDX

Fig. 5 presents the micrographs displaying clearly the interfaces of SFMO-LSGM and BSCF-LSGM and the SFMO anode surface. As shown in Fig. 5(a), the SFMO anode and the LSGM electrolyte match very well and the thickness of the SFMO phase is about 55 μm. Fig. 5(b) demonstrates the surface of the SFMO anode with a uniform size distribution of the particles and pores with grain sizes ranging from 2 to 4 μm. Fig. 5(c) indicates that there exists some incomplete combination between the BSCF cathode and the LSGM electrolyte phases, which may comes from the thermal expansion incompatibility between BSCF cathode and the electrolyte (the TEC value of BSCF is $19.2 \times 10^{-6}\,K^{-1}$ in air [37] while that of LSGM is $11.7 \times 10^{-6}\,K^{-1}$ in N_2). The thickness of the BSCF cathode is about 24 μm.

The EDX linear scanning result of the interface between SFMO and LSGM phases after the cell performance measurement is shown in Fig. 6. No obvious La signal is observed in the anode region, indicating that there is no interdiffusion of La between the anode and the electrolyte, so that no any buffer layer like LDC is needed in this single cell.

3.5. Single cell performance

The LSGM electrolyte supported single fuel cell with the configuration of SFMO|LSGM|BSCF was tested using H_2 and dry CH_4 as the fuel, respectively, and O_2 as the oxidant. Before testing, the anode was exposed to H_2 at 850 °C for 5 h to ensure the double-perovskite structure and then supplied with fuel gas. Fig. 7(a)

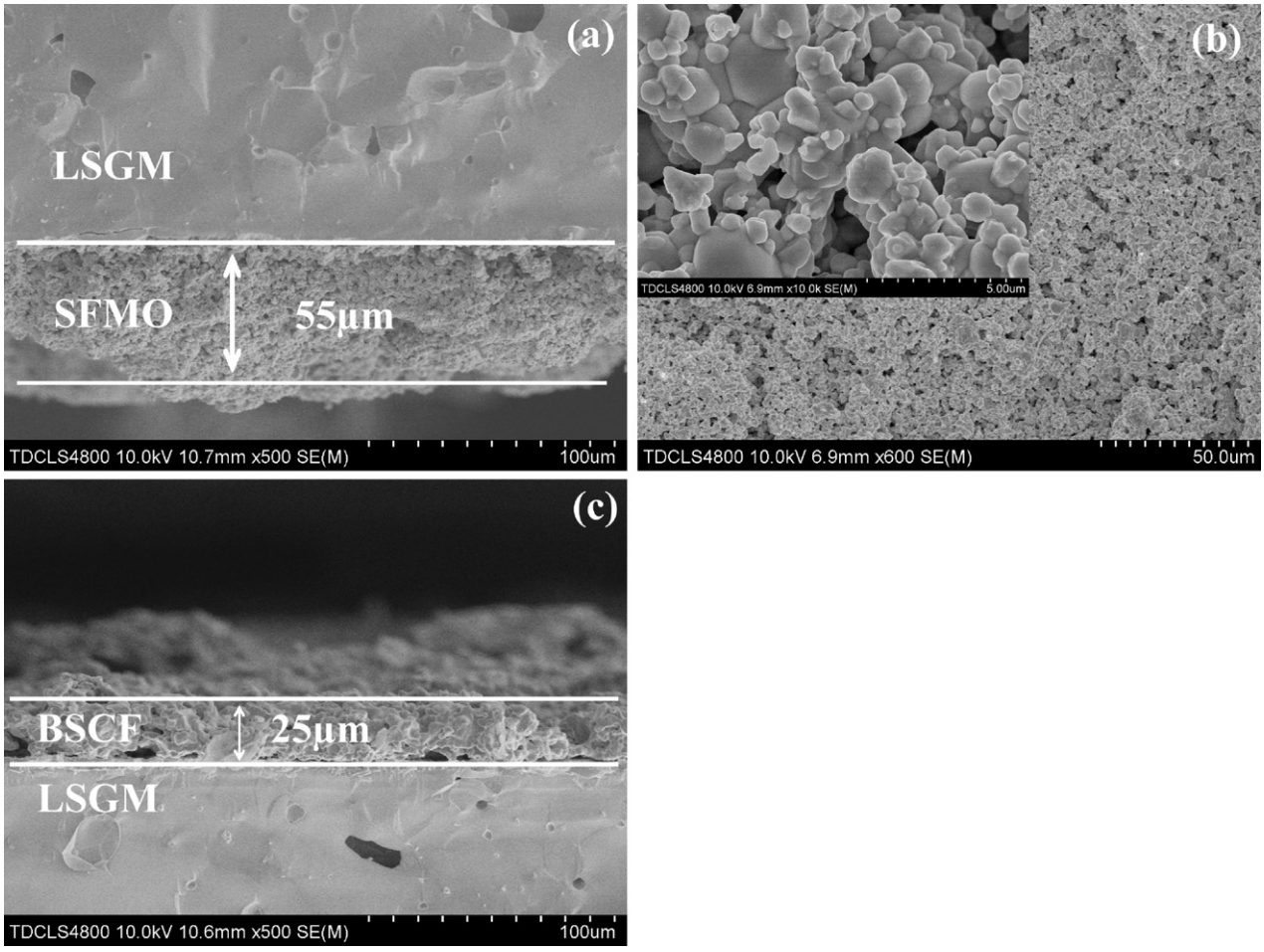

Fig. 5. SEM images taken before the cell test: (a) anode and electrolyte interface, (b) surface of the SFMO anode, and (c) cathode and electrolyte interface.

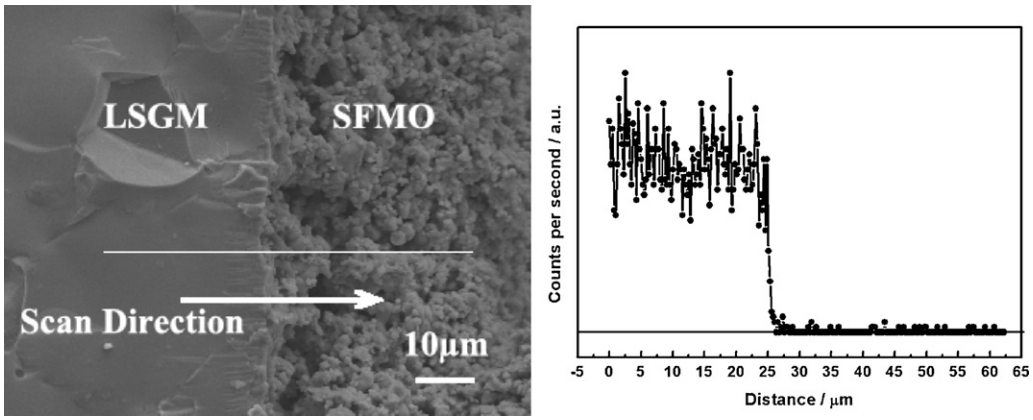

Fig. 6. EDX linear scanning of the tested single cell, the right figure indicates that there is no interdiffusion of La between the anode and the electrolyte.

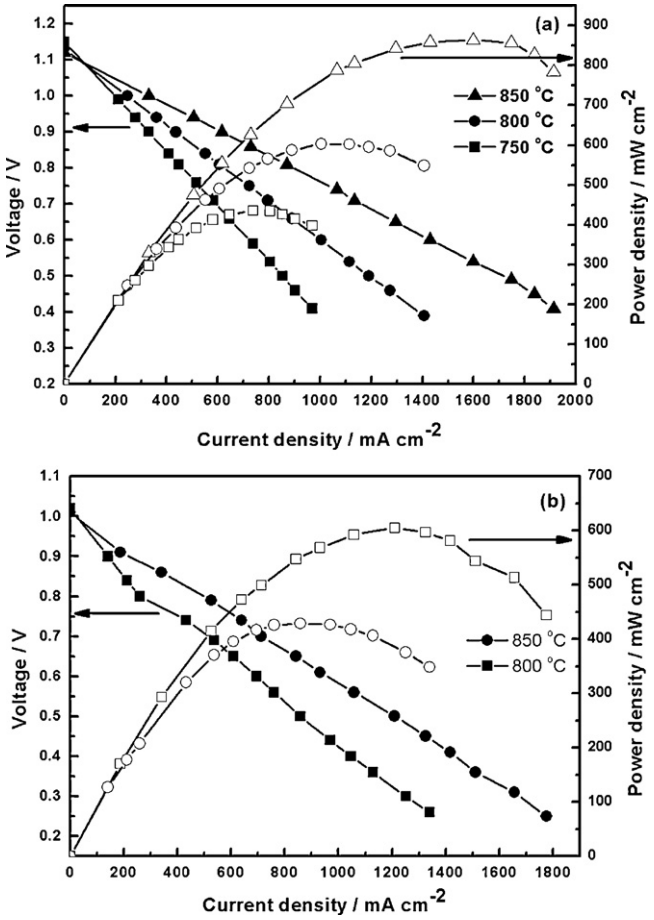

Fig. 7. SFMO|LSGM|BSCF cell voltage and power density as a function of current density in (a) H_2 and (b) dry CH_4.

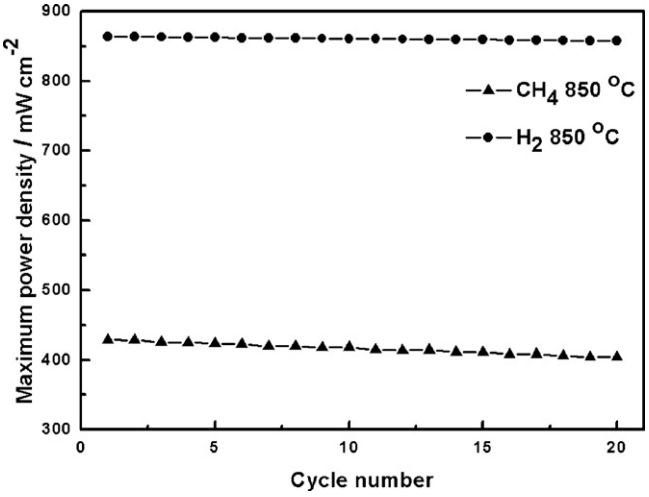

Fig. 8. P_{max} at 850 °C as a function of the cycle numbers in H_2 and dry CH_4.

shows plots of the power densities and voltages as functions of the current density and working temperature for H_2 fuel. The cell exhibited maximum power densities (P_{max}) of 863.8 mW cm^{-2}, 603.2 mW cm^{-2} and 435.6 mW cm^{-2} at 850 °C, 800 °C and 750 °C, respectively. For the dry CH_4 as the fuel, the P_{max} of the single cell reached 604.8 mW cm^{-2} and 429.1 mW cm^{-2} at 850 and 800 °C, respectively as shown in Fig. 7(b). These results are much higher than SOFCs using rare-earth doped ceria impregnated with CuO or LSCM [3,25]. When comparing to Huang's result, their data showed Sr_2MgMoO_6 gives a power out of 438 mW cm^{-2} at 800 °C with dry CH_4 as fuel [28,29], so SFMO gives a similar performance to Sr_2MgMoO_6. But we have to notice that the performance of the SOFC is not only controlled by anode, but also by other factors such as conductivity of electrolyte, activity of cathode, etc., which means the results are not very comparable except other components are all the same.

As the anode has different degradation potential at different output current density [38,39], in order to clearly show the stability of the SFMO double-perovskite material during the whole power generation cycle, we run the cell for repeated power cycles at 850 °C with H_2 or CH_4 as fuels and the P_{max} in each cycle was recorded. Fig. 8 presents the P_{max} in each cycle as a function of the cycle numbers for H_2 and CH_4 fuels. It shows that P_{max} fades by 0.7% in H_2 fuel and 5.7% in dry CH_4 fuel over 20 cycles, respectively. These results indicate that SFMO exhibits a stable performance in H_2 fuel and has a much better stability than the often used Ni-based anodes in dry CH_4 fuel.

4. Conclusion

A double-perovskite oxide SFMO has been synthesized by a combined citrate-EDTA complexing technique and used as the anode material of a SOFC. The XRD analysis results indicate that a pure double-perovskite phase is obtained by reducing the synthesized powder at 1100 °C in 5%H_2/Ar for 20 h, the double-perovskite structure can be destroyed by calcination in air at the same temperature but the structure can be restored by heating in H_2 at 850 °C again. XPS data show the co-existence of Fe^{3+}–Mo^{5+} and Fe^{2+}–Mo^{6+}

pairs in the double-perovskite structure, which may be the origin of the high catalytic activity in H_2 and CH_4. TEC value of SFMO double-perovskite material is $14.0 \times 10^{-6}\,K^{-1}$ in N_2, which is close to that of LSGM ($11.7 \times 10^{-6}\,K^{-1}$).

A single cell with SFMO as the anode material has been constructed using LSGM and BSCF as the electrolyte and the cathode material, respectively. EDX analysis of the SFMO-LSGM interface in the tested single cell indicates that there is no conspicuous inter-diffusion of the ionic species. The single cell exhibits a maximum power density of 863.7 mW cm^{-2} in H_2 and 604.8 mW cm^{-2} in CH_4 at 850 °C, respectively. The durability test of the single cell tells that SFMO exhibits a more stable performance in dry CH_4 atmosphere than the often reported Ni based anode materials in literature.

All these experimental results indicate that the SFMO double-perovskite material has a great potential for using as the anode material in intermediate temperature SOFCs both with H_2 and CH_4 as the fuels.

Acknowledgements

The financial support of NSF of China under contract numbers 21076150 and 20736007 are gratefully acknowledged. The work has been also supported by the Program of Introducing Talents to the University Disciplines under file number B06006, and the Program for Changjiang Scholars and Innovative Research Teams in Universities under file number IRT 0641.

References

[1] N.Q. Minh, Solid State Ionics 174 (2004) 271–277.
[2] E.P. Murray, T. Tsai, S.A. Barnett, Nature 400 (1999) 649–651.
[3] S. Park, J.M. Vohs, R.J. Gorte, Nature 404 (2000) 265–267.
[4] H. Kim, S. Park, J.M. Vohs, R.J. Gorte, J. Electrochem. Soc. 148 (2001) A693–A695.
[5] A. Weber, B. Sauer, A.C. Muller, D. Herbstritt, E. Ivers-Tiffee, Solid State Ionics 152–153 (2001) 543–550.
[6] R.J. Gorte, H. Kim, J.M. Vohs, J. Power Sources 106 (2002) 10–15.
[7] S. McIntosh, R.J. Gorte, Chem. Rev. 104 (2004) 4845–4865.
[8] L.J. Jia, Y. Tian, Q.H. Liu, C. Xia, J.S. Yu, Z.M. Wang, Y.C. Zhao, Y.D. Li, J. Power Sources 195 (2010) 5581–5586.
[9] C.M. Finnerty, R.M. Ormerod, J. Power Sources 86 (2000) 390–394.
[10] B.C.H. Steele, A. Heinzel, Nature 414 (2001) 345–352.
[11] P.N. Huang, A. Petric, J. Electrochem. Soc. 143 (1996) 1644–1648.
[12] C. Xia, Y. Li, Y. Tian, Q.H. Liu, Z.M. Wang, L.J. Jia, Y.C. Zhao, Y.D. Li, J. Power Sources 195 (2010) 3149–3154.
[13] R. Pelosato, I. Natali Sora, V. Ferrari, G. Dotelli, C.M. Mari, Solid State Ionics 175 (2004) 87–92.
[14] B. Zhu, Int. J. Energy Res. 30 (2006) 895–903.
[15] Y.D. Li, Z.B. Rui, C. Xia, M. Anderson, Y.S. Lin, Catal. Today 148 (2009) 303–309.
[16] C. Xia, Y. Li, Y. Tian, Q.H. Liu, Y.C. Zhao, Y.D. Li, J. Power Sources 188 (2009) 156–162.
[17] Z.P. Shao, S.M. Haile, Nature 431 (2004) 170–173.
[18] M. Ihara, C. Yokoyama, A. Abudula, R. Kato, H. Komiyama, K. Yamada, J. Electrochem. Soc. 146 (1999) 2481–2487.
[19] Y. Matsuzaki, I. Yasuda, Solid State Ionics 132 (2000) 261–269.
[20] S. McIntosh, J.M. Vohs, R.J. Gorte, Electrochem. Solid State 6 (2003) A240–A243.
[21] S. Park, R. Craciun, J.M. Vohs, R.J. Gorte, J. Electrochem. Soc. 146 (1999) 3603–3605.
[22] H. Kim, C. Lu, W.L. Worrell, J.M. Vohs, R.J. Gorte, J. Electrochem. Soc. 149 (2002) A247–A250.
[23] E. Nikolla, J. Schwank, S. Linic, J. Electrochem. Soc. 156 (2009) B1312–B1316.
[24] Y.B. Lin, Z.L. Zhan, S.A. Barnett, J. Power Sources 158 (2006) 1313–1316.
[25] S.W. Tao, J.T.S. Irvine, Nat. Mater. 2 (2003) 320–323.
[26] S.W. Zha, P. Tsang, Z. Cheng, M.L. Liu, J. Solid State Chem. 178 (2005) 1844–1850.
[27] J. Wan, J.H. Zhu, J.B. Goodenough, Solid State Ionics 177 (2006) 1211–1217.
[28] Y.H. Huang, R.I. Dass, J.C. Denyszyn, J.B. Goodenough, J. Electrochem. Soc. 153 (2006) A1266–A1272.
[29] Y.H. Huang, R.I. Dass, Z.L. Xing, J.B. Goodenough, Science 312 (2006) 254–257.
[30] Y.H. Huang, G. Liang, M. Croft, M. Lehtimaki, M. Karppinen, J.B. Goodenought, Chem. Mater. 21 (2009) 2319–2326.
[31] J. Linden, T. Yamamoto, M. Karppinen, H. Yamauchi, T. Pietari, Appl. Phys. Lett. 76 (2000) 2925–2927.
[32] T.T. Fang, M.S. Wu, T.F. Ko, J. Mater. Sci. Lett. 20 (2001) 1609–1610.
[33] H. Falcón, J.A. Barbero, G. Araujo, M.T. Casais, M.J. Martínez-Lope, J.A. Alonso, J.L.G. Fierro, Appl. Catal. B 53 (2004) 37–45.
[34] Z.P. Shao, W.S. Yang, Y. Cong, H. Dong, J.H. Tong, G.X. Xiong, J. Membr. Sci. 172 (2000) 177–188.
[35] M. Mori, N.M. Sammes, Solid State Ionics 146 (2002) 301–312.
[36] M. Retuerto, F. Jimenez-Villacorta, M.J. Martinez-Lope, Y. Huttel, E. Roman, M.T. Fernandez-Diaz, J.A. Alonso, Phys. Chem. Chem. Phys. 12 (2010) 13616–13625.
[37] Q.S. Zhu, T.A. Jin, Y. Wang, Solid State Ionics 177 (2006) 1199–1204.
[38] X. Zhang, S. Ohara, H. Chen, T. Fukui, Fuel 81 (2002) 989–996.
[39] T. Matsui, T. Iida, M. Kawano, T. Inagaki, R. Kikuchi, K. Eguchi, ECS Trans. 7 (2007) 1437–1445.